(Received 25 September 2025, Accepted 11 November 2025, Scheduled 19 December 2025)

Experimental Results and Analysis of a 2-Receiver Midrange Wireless Power Transfer System in Seawater

Xiaoliang Li, Wangqiang Niu*, and Xianwen Zhou

Key Laboratory of Transport Industry of Marine Technology and Control Engineering
Shanghai Maritime University, Shanghai 201306, China

ABSTRACT: Due to the high electrical conductivity, relative permittivity, and magnetic permeability of seawater, the propagation behavior of electromagnetic fields differs significantly from that in air. The conductive nature of seawater causes strong eddy current loss and magnetic field attenuation, thereby reducing the effective coupling coefficient and resulting in frequency detuning between the transmitter and receiver coils. Moreover, the marine environment introduces parasitic impedance paths and additional energy dissipation due to the conductive medium, which further decreases transmission efficiency. These unique electromagnetic characteristics make the design and optimization of wireless power transfer (WPT) systems in seawater more complex and challenging than in air, motivating this study to develop and analyze a dual-receiver WPT architecture that improves midrange transmission efficiency under underwater conditions. To address this issue, a single-transmitter dual-receiver (1TX-2RX) WPT system operating in the 300–550 kHz frequency range is designed and implemented. Experimental results demonstrate that, under midrange transmission in seawater, the efficiency of the proposed 2RX architecture improves markedly from 12% in the 1RX system to 25%, while maintaining stable output performance under various receiver coil misalignment conditions. In addition, compared with operation in air, the optimal operating frequency of the 2RX system in seawater shifts leftward from approximately 460 kHz to 410 kHz. To better characterize the impact of seawater on transmission performance, complex impedance and mutual inductance parameters are incorporated into the conventional circuit model, enabling effective representation of the additional losses and coupling attenuation induced by the conductive medium. The predicted load voltage is consistent largely with the experimental measurements, validating the accuracy and applicability of the proposed modeling approach. Overall, this study not only experimentally verifies the feasibility of improving midrange transmission efficiency through a dual-receiver architecture but also establishes theoretically a circuit modeling method suited better for seawater environments, providing useful insights for the design and optimization of marine WPT systems.

1. INTRODUCTION

Wireless Power Transfer (WPT) has been widely adopted in various industries, including medical, aerospace, and home appliances, as well as underwater devices that require specialized power supplies, due to its non-contact power transmission capabilities [1]. Traditional underwater devices, such as autonomous underwater vehicles (UUVs), are typically powered through conventional cables or batteries, and the batteries should be recharged or replaced regularly, which greatly affects their operational range, stability, and concealment, especially in special underwater missions [2].

In the air, traditional series-series (S-S) wireless power transfer systems exhibit a significant decline in transmission efficiency as the distance increases under mid-range conditions, primarily due to severe power attenuation. Common approaches to improve efficiency include adding extra transmitter coils or relay coils to reduce energy loss [3], or incorporating ferrite materials to enhance magnetic coupling between coils [4]. However, unlike air, seawater presents unique physical properties such as high conductivity and permittivity. Under such conditions, applying the same strategies — such as adding transmitter coils or ferrite materials — may lead to an increase in the equivalent series resistance of the system, thereby increasing energy losses and negatively impacting overall efficiency [5]. Therefore, there is an urgent need to carry out a systematic and in-depth study on the transmission topology of wireless power transfer systems to improve the overall transmission performance and efficiency [6].

Unlike air, seawater, as a medium with high conductivity, has an important impact on the transmission characteristics of WPT systems [7]. Several researches have explored the transfer ability of multi-receiver WPT systems in the air. Ref. [8] verified the feasibility of a single transmission coil under multi-load conditions by expanding it into two small transmission coils by experimental means. Still, it did not provide an in-depth theoretical analysis of the transmission mechanism and system characteristics. Ref. [9] investigated the multiple resonant coil structure and showed that the introduction of an intermediate resonant coil helps to extend the transmission distance; however, it did not consider the effect of the relative position between the pickup coil and the resonant coil on the system performance. Ref. [10] proposes a wireless power transfer system based on a dual pickup coil structure, which can significantly improve the output power and transmission efficiency of a WPT system under heavy load conditions. However, the

* Corresponding author: Wangqiang Niu (wqniu@shmtu.edu.cn).

performance enhancement of this scheme is realized based on the prerequisite of neglecting the mutual inductance between the receiving coils.

Currently, WPT systems in seawater environments still face many technical challenges, including eddy current losses caused by the conductive medium, the splitting phenomenon of the resonant frequency [11], the rapid attenuation of the magnetic field in seawater, and the system stability problem caused by the ocean current perturbation [12]. Ref. [13] presents a Z-parameters method for efficient modeling of underwater wireless energy transmission based on impedance parameters. The method combines electromagnetic field analysis and two-port network theory, and establishes a coil impedance model that includes the effects of seawater medium properties, thus more accurately describing the electromagnetic behavior of coils in underwater environments. Ref. [14] designs and realizes a wireless magnetic resonance power transmission system with a multi-coil structure based on the theory of Band-Pass Filter (BPF). The system optimizes the coupling characteristics between the coils through the filter theory, which improves the energy transmission efficiency and system stability. Ref. [15] simplifies the modeling and analysis of eddy current losses by equating the eddy current effect induced by the time-varying electromagnetic field in seawater to two additional resistors connected in series to the primary and secondary side coils. Ref. [16] pointed out that in a uniform dissipative medium, there is a significant electromagnetic coupling between the driving current and the induced eddy currents, and this interaction will cause changes in the self-impedance of the coils and their mutual inductance with each other, which will have an important effect on the electromagnetic characteristics of the wireless energy transmission system. Ref. [17] experimentally found that the transmission efficiency of a symmetric WPT system in seawater is significantly higher than in air under midrange transmission conditions (where the transmission distance exceeds the outer diameter of the transceiver coils) and a triple-coil coupling circuit model is proposed to explain their observations. Ref. [18] proposed a Multi-Transmitter Multi-Receiver (MT-MR) WPT system and combined it with a maximum efficiency tracking algorithm, which was successfully applied to an underwater buoy platform. The system can wirelessly charge multiple beacon devices at the same time, thus supporting more data transmission tasks and improving the overall performance and operational efficiency of the underwater communication system. Ref. [19] proposes a modeling method based on complex self- and complex-mutual inductance to explain phenomena such as transmission efficiency enhancement and optimal frequency left-shift in a midrange seawater environment. The study finds the trend of the real part of the complex mutual inductance increasing with frequency and points out that this trend is an important reason leading to the enhancement of the system's transmission capability, which provides a good reference for the complex impedance modeling of the single-transmitter-dual-receiver system investigated in this paper.

In this paper, experiment is platformed for a 1TX-1RX and a 1TX-2RX system are first constructed based on the classical series-series (S-S) topology, and experimental observations are carried out in both air and seawater environments. The experimental results show that the maximum load voltage of the 1TX-2RX system in seawater is also left-shifted compared with that in air, and the performance is similar to that of the 1TX-1RX system; moreover, the load voltage and transmission efficiency of the 1TX-2RX system in seawater are better than those in air environment at midrange. In addition, the transmission efficiency was significantly improved from 12% (in the 1RX system) to 25% (in the 2RX system). It is also found that in seawater, when the receiving coil is offset within 15 cm relative to the transmitting coil, the load voltage of the 2RX system is less affected; the transmission performance remains stable; and the system has better anti-offset characteristics. Finally, inspired by [13–16], a new circuit model containing complex impedance and complex mutual inductance parameters is proposed to describe the transmission behavior of the 1TX-2RX system in seawater, and the model is verified by experiments.

This paper is divided into five parts. The first part reviews and summarizes the previous research in related fields. The second part builds an underwater experimental platform and shows the experimental results. The third part proposes a new circuit model for the experimental results and analyzes the parameters in the model in detail. The fourth part provides a theoretical explanation of the experimental results based on this circuit model. Finally, Part V summarizes the whole paper.

2. EXPERIMENTS ON WPT SYSTEMS IN AIR AND SEAWATER

2.1. Experimental Platform Construction

A 1TX-1RX WPT system is first analyzed, which serves as a theoretical and experimental reference for the proposed 1TX-2RX WPT system.

2.1.1. Circuit Model of the 1RX and 2RX System in Air

(1) 1TX-1RX WPT system

For a typical WPT system with S-S topology, the circuit topology is shown in Fig. 1. The dot convention for mutual inductances is applied in the equivalent circuit diagram to indicate the polarity of the coupling between coils, ensuring that the additive or differential nature of mutual inductance is clearly defined.

The parameters of the1TX-1RX system in the air are shown in Table 1. The circuit parameters listed in Table 1, including resistances, inductances, and capacitances, are measured experimentally in the laboratory. The mutual inductance between coils changes with the transmission distance. Since this work focuses on the midrange (30 cm) underwater wireless power transfer condition, only the simulated mutual inductance calculated by ANSYS Maxwell at 30 cm in air are listed in Table 1.

(2) 1TX-2RX WPT system

The circuit topology of the 1TX-2RX WPT system is shown in Fig. 2. Two receiving coils are connected in series to the same load, where the dot convention is applied to indicate the polarity of mutual inductances.

TABLE 1. Experimental parameters of the 1RX WPT system in air.

Parameter	Symbol	Value
R_1	Equivalent internal resistance of primary/Ω	0.35
R_2	Equivalent internal resistance of secondary side circuit/Ω	0.32
R_L	Secondary side load resistance/Ω	20
R_B	Primary side balancing resistance/Ω	20
C_1, C_2	Compensation capacitor/nF	2
L_1, L_2	Coil Equivalent Inductance/μH	64
$\dot{U}_{in}$	High Frequency Voltage Sources/V	20
M_{12}	Mutual inductance (30 cm)/μH	0.937

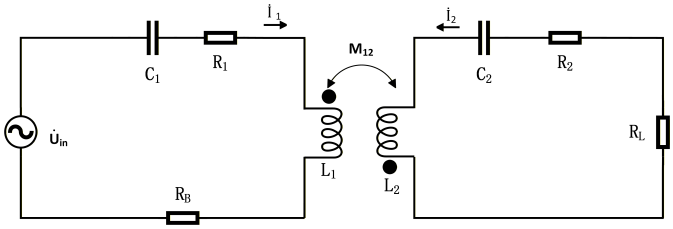

FIGURE 1. 1TX-1RX WPT system circuit topology in air.

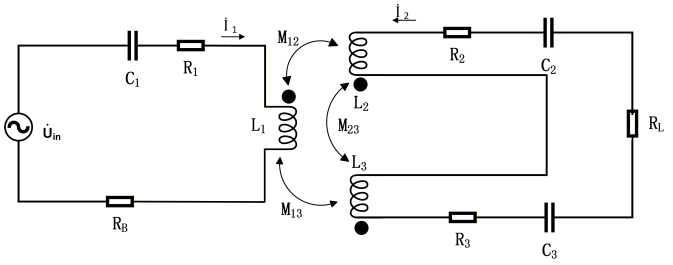

FIGURE 2. 1TX-2RX WPT system circuit topology in air.

The parameters of the 1TX-2RX system in air are shown in Table 2 Among them, M12 and M13 represent the mutual inductances between the coils, and M12 = M13 at a transmission distance of 30 cm is calculated by ANSYS Maxwell, and other parameters are measured experimentally in the laboratory.

2.1.2. Construction of WPT Experimental Platform in Seawater

Based on the circuit topologies of the 1RX and 2RX configurations in air, experimental platforms were designed for both air and seawater environments, as illustrated in Fig. 3. The main circuits of the 1TX-1RX and 1TX-2RX wireless power transfer systems primarily consist of coils, resistors, and compensation capacitors. The coils are wound with AWG16 copper wire in 17 turns, featuring an inner diameter of 12 cm and an outer diameter of 22 cm. To simulate the seawater environment, the coils are immersed in a water tank with dimensions of $120 \times 70 \times 70$ cm^3, into which sea salt is dissolved. The conductivity of the prepared seawater is 3.41 S/m at room temperature (20°C), measured using a conductivity meter (LC-DDB-1A, Shanghai Lichen Bangxi).

TABLE 2. 2RX WPT system experimental parameters in air.

Parameter	Symbol	Value
R_1	Equivalent internal resistance of primary/Ω	0.35
R_2	Equivalent internal resistance of secondary side circuit/Ω	0.32
R_L	Secondary side load resistance/Ω	20
R_B	Primary side balancing resistance/Ω	20
C_1, C_2, C_3	Compensation capacitor/nF	2
L_1, L_2, L_3	Coil Equivalent Inductance/μH	64
$\dot{U}_{in}$	High Frequency Voltage Sources/V	20
M_{12}, M_{13}	Mutual inductance (30 cm)/μH	1.38

Figure 4 illustrates the experimental setup, including a signal generator (Tektronix AFG3102), a 10 W power amplifier (Rigol PA1011), and an oscilloscope (Rigol DS1302). The signal generator outputs a sinusoidal waveform, which is amplified tenfold by the power amplifier and then fed into the transmitter coil. In addition, Fig. 4 shows the load voltage waveform of the 1TX-1RX WPT system in air at a transmission distance of 30 cm, with the resonant frequency set to 500 kHz.

2.2. Experimental Observations in Air and Seawater

Based on the obtained circuit parameters, experimental tests were conducted for both single-receiver 1RX and 2RX systems in air and seawater environments. The comparative experimental results are presented as follows.

2.2.1. Performance of 1RX and 2RX Systems in Air (Without Misalignment)

As shown in Fig. 5, the load voltage of both systems initially increases and then decreases with increasing frequency in air, reaching a peak near the resonant frequency under a fixed transmission distance. Moreover, the load voltage declines as the transmission distance increases. In short-range transmission, the single-receiver system exhibits frequency splitting due to over-coupling between the coils [20], whereas the dual-receiver system remains relatively stable.

2.2.2. Performance of 1RX and 2RX Systems in Seawater (Without Misalignment)

In seawater, the 1RX system exhibits frequency splitting at close transmission distances, resulting in multiple peaks in the load voltage response. In contrast, the 2RX system remains stable under the same conditions, showing no signs of frequency splitting as shown in Fig. 6. At midrange transmission distances, both systems demonstrate relatively stable performance without frequency splitting. Furthermore, the 2RX system maintains a more consistent load voltage under midrange conditions, whereas the 1RX system shows a noticeable voltage drop. Similar experimental observations have also been reported in the literature [21], where the SEPIC-controlled 1RX

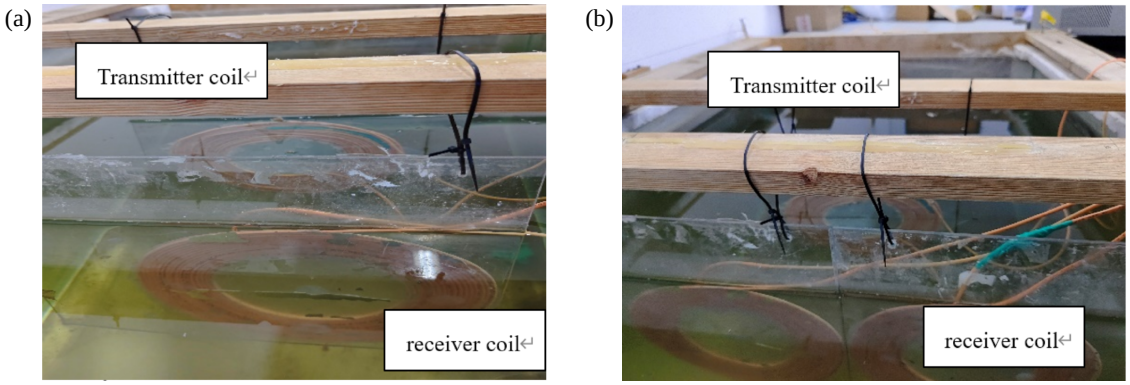

FIGURE 3. Underwater wireless power transfer experimental platform: (a) single transmitter, single receiver; (b) single transmitter, double receiver.

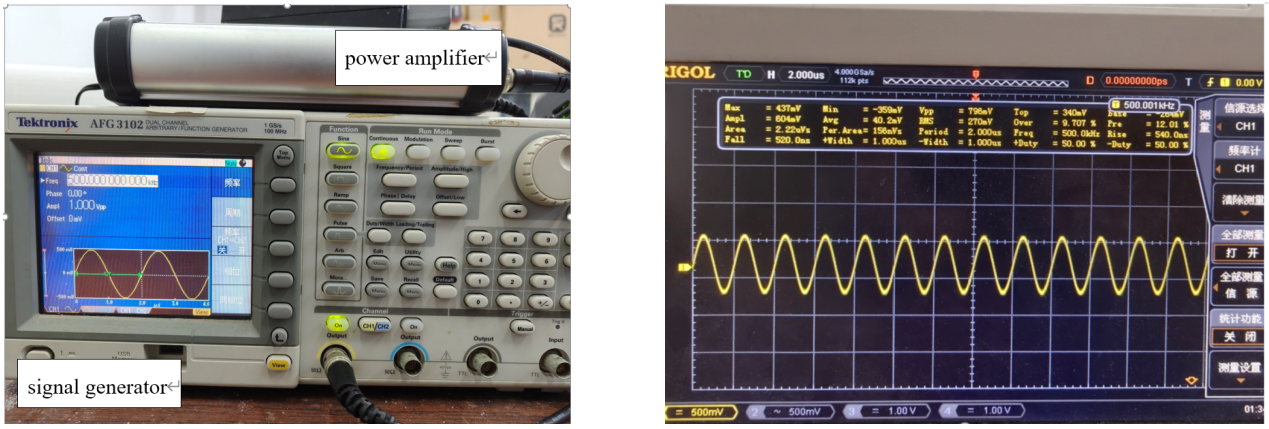

FIGURE 4. The power amplifier, the signal generator and the oscilloscope.

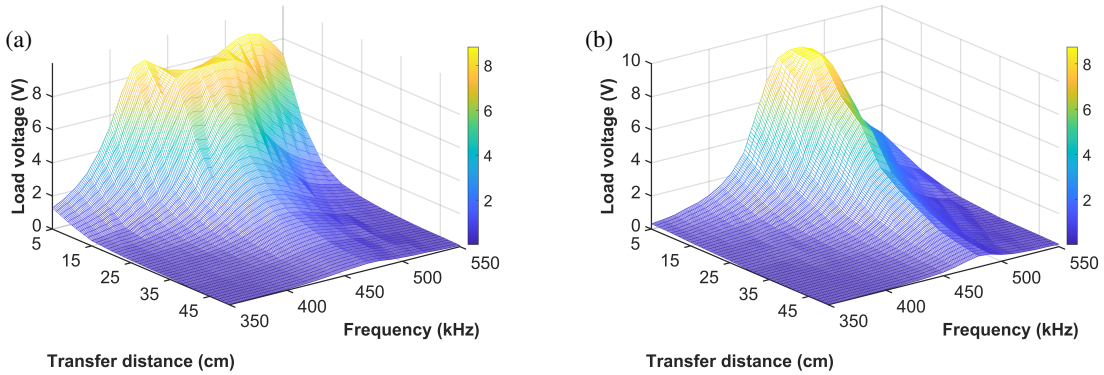

FIGURE 5. Experimental load voltage in air for (a) 1RX and (b) 2RX WPT systems at different transmission distances and frequencies.

WPT system in seawater maintains a stable output under different offsets and angular variations.

2.2.3. Performance of 1RX and 2RX Systems in Seawater (With Misalignment)

Given the complexity of the seawater environment, transmitter-receiver coil misalignment may occur during operation. In this experiment, the transmission distance was fixed at 30 cm to simulate a midrange scenario, while introducing lateral misalignment by offsetting the receiver coil from the transmitter coil. The offset distance was varied from 0 cm to 15 cm in 5 cm increments.

The variation of load voltage with frequency under different offset distances is shown in Fig. 7. It can be observed that the load voltage remains relatively stable despite changes in offset distance, indicating that the 2RX is less affected by positional deviation.

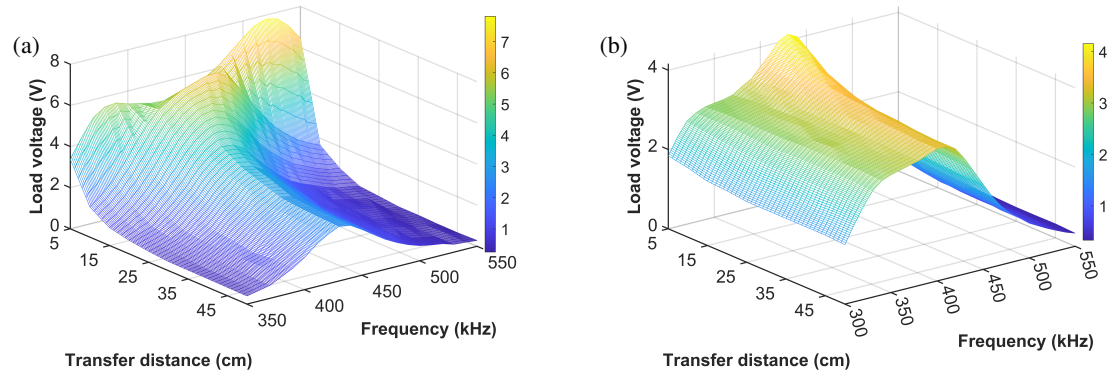

FIGURE 6. Experimental load voltage for (a) 1RX and (b) 2RX in seawater at different transmission distances and frequencies.

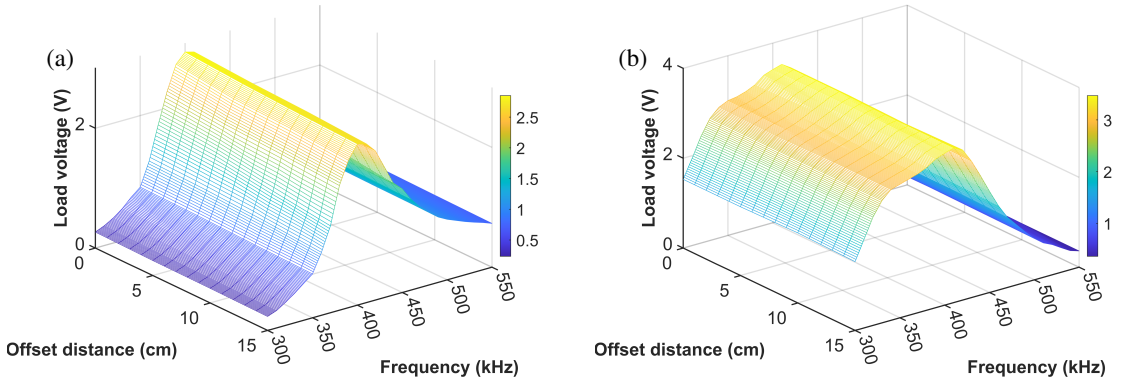

FIGURE 7. Experimental load voltage in seawater (a) 1RX; (b) 2RX at different offset distances and frequencies.

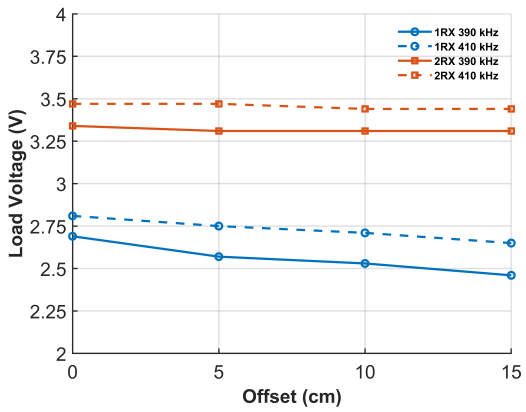

FIGURE 8. Experimental load voltage of the 2RX&1RX system at different offsets in seawater.

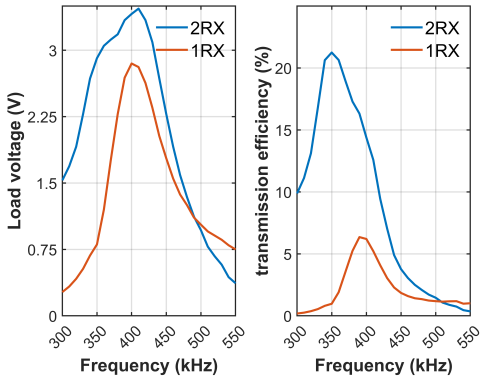

FIGURE 9. Comparison of the Experimental load voltage and transmission efficiency between 2RX and 1RX systems in seawater.

In addition, load voltage variations of the 1RX and 2RX systems were compared at fixed frequencies of 390 kHz and 410 kHz under different offset distances. As shown in Fig. 8, the 2RX system exhibits smaller voltage fluctuations with increasing misalignment compared to the 1RX, indicating better stability under offset conditions.

2.2.4. Efficiency Comparison between 1RX and 2RX Systems in Seawater (Midrange)

Under a midrange transmission distance of 30 cm, the output voltages and transmission efficiencies of 1RX and 2RX WPT systems are compared in a seawater environment with a 20 Ω load. As shown in Fig. 9, the 2RX system delivers a higher load voltage and a better transmission efficiency, increasing from 12% in the 1RX configuration to 25% in the 2RX setup.

Overall, compared to the 1RX system, the 2RX configuration demonstrates improved load voltage and transmission efficiency under midrange transmission conditions. Moreover, it exhibits better stability in the presence of misalignment between the transmitting and receiving coils.

3. CIRCUIT MODELING OF THE 2RX SYSTEM IN AIR AND SEAWATER

In this section, the circuit model of the underwater WPT system is established, followed by an investigation of its transmission characteristics under midrange conditions.

3.1. Circuit Model of the 2RX System in Air

The 1TX-2RX WPT circuit model in air is shown in Fig. 2. Two receiving coils are connected in series to the same load.

According to Kirchhoff's voltage law, the equation for the 1TX-2RX configuration is:

$$\begin{bmatrix} \dot{U}_{in} \\ 0 \end{bmatrix} = \begin{bmatrix} Z_{1\_air} & j\omega\left(M_{12}+M_{13}\right) \\ j\omega\left(M_{12}+M_{13}\right) & Z_{2\_air} \end{bmatrix} \cdot \begin{bmatrix} \dot{I}_1 \\ \dot{I}_2 \end{bmatrix} \quad (1)$$

where:

$$Z_{1\_air} = R_{\mathrm{B}}+R_1+\mathrm{j}\omega L_1+\frac{1}{\mathrm{j}\omega C_1} \quad (2)$$

$$Z_{2\_air} = R_{\mathrm{L}}+R_2+R_3+\mathrm{j}\omega(L_2+L_3)+\frac{1}{\mathrm{j}\omega(C_2+C_3)} \quad (3)$$

Similar to the 1RX system, the circuit impedance in the 2RX system becomes purely resistive at resonance, resulting in maximum active power transfer. To ensure circuit symmetry, structural consistency, and ease of calculation, the primary and secondary sides are designed to operate at the same resonant frequency, satisfying the following condition: $L_1 = L_2 = L_3$; $C_1 = C_2 = C_3$.

From Equation (1), the current of the primary and secondary side circuits is found to be:

$$\begin{cases} \dot{I}_{1\_air} = \frac{\dot{U}_{in}Z_{2\_air}}{\omega^2(M_{12}+M_{13})^2+Z_{1\_air}Z_{2\_air}} \\ \qquad\quad = \frac{\dot{U}_{in}}{Z_{1\_air}+\frac{(\omega(M_{12}+M_{13}))^2}{Z_{2\_air}}} \\ \dot{I}_{2\_air} = \frac{\omega(M_{12}+M_{13})\dot{U}_{in}}{\omega^2(M_{12}+M_{13})^2+Z_{1\_air}Z_{2\_air}} \end{cases} \quad (4)$$

Let $Z_{ref} = \frac{(\omega M_{12}+M_{13})^2}{Z_{2\_air}}$ be the reflected impedance on the secondary side.

The equivalent total impedance on the primary side is:

$$Z_{in\_air} = Z_{1\_air}+\frac{\left(\omega(M_{12}+M_{13})\right)^2}{Z_{2\_air}} \quad (5)$$

The input power of the system is:

$$P_{in} = \frac{U_{in}^2 Z_2}{\omega^2\left(M_{12}+M_{13}\right)^2+Z_{1\_air}Z_{2\_air}} \quad (6)$$

The output power of the system is:

$$P_{out} = \frac{\left(\omega(M_{12}+M_{13})\,U_{in}\right)^2 R_L}{\left[\omega^2\left(M_{12}+M_{13}\right)^2+Z_{1\_air}Z_{2\_air}\right]^2} \quad (7)$$

The System efficiency is:

$$\eta = \frac{P_{in}}{P_{out}} = \frac{\dot{I}_{2\_air}^2 R_L}{\mathrm{U_{in}}\dot{I}_{2\_air}} \quad (8)$$

When the input voltage and load of the system are fixed, the transmission efficiency is primarily determined by the currents on the primary and secondary sides. Define the current ratio as $\alpha = \frac{\dot{I}_{2\_air}}{\dot{I}_{1\_air}}$, a larger α indicates a higher efficiency η; Under resonance conditions, $\mathrm{j}\omega L+\frac{1}{\mathrm{j}\omega \mathrm{C}} = 0$ holds, the maximum transmission efficiency can be simplified as:

$$\eta_{\max} = \frac{\omega^2(M_{12}+M_{13})^2 R_L}{(R_2+R_3+R_L)\times\left[(R_{\mathrm{B}}+R_1)\right.} \\ \left.(R_2+R_3+R_L)+\omega^2(M_{12}+M_{13})^2\right] \quad (9)$$

3.2. Circuit Model of the 2RX System in Seawater

The circuit model of the 2RX system in seawater is developed based on the previously established dual-receiver model in the air. Since the two receiver coils are connected in series and have identical circuit parameters, the impedance variation caused by seawater is denoted collectively as ΔZ.

To simplify the analysis, the mutual inductance between the transmitting coil and the two receiver coils in seawater is uniformly defined as M_{sea}. The high electrical conductivity of seawater alters the equivalent parameters of the coils, thereby affecting the magnetic coupling characteristics and power transfer efficiency.

It has been shown that the complex mutual inductance between coils in underwater environments exhibits nonlinear variation with frequency and introduces additional eddy current losses and phase delay [22]. In [23], a frequency-domain coupled model incorporating complex impedance and mutual inductance was developed based on both electromagnetic simulations and experimental data, providing a solid theoretical foundation for the modeling approach used in this study. The circuit model of the 2RX system in seawater is illustrated in Fig. 10, where the dot convention is used to represent the polarity of mutual inductances between coils.

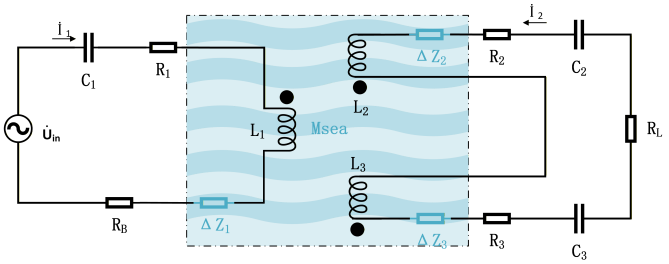

FIGURE 10. Single Transmitter dual receiver underwater circuit topology.

From Kirchhoff's voltage law, the circuit equation can be obtained as:

$$\begin{bmatrix} \dot{U}_{in} \\ 0 \end{bmatrix} = \begin{bmatrix} Z_{1_{sea}}+\Delta Z_1 & j\omega M_{sea} \\ j\omega M_{sea} & Z_{2\_sea}+\Delta Z_2+\Delta Z_3 \end{bmatrix} \cdot \begin{bmatrix} \dot{I}_1 \\ \dot{I}_2 \end{bmatrix} \quad (10)$$

where the complex impedance is $\Delta Z_1 = \Delta Z_2 = \Delta Z_3$, and Msea is the complex mutual inductance between the coils in seawater.

$$\begin{cases} Z_{1\_sea} = R_{\mathrm{B}} + R_1 + \mathrm{j}\omega L_1 + \frac{1}{\mathrm{j}\omega C_1} \\ Z_{2\_sea} = R_{\mathrm{L}} + R_2 + R_3 + \mathrm{j}\omega(L_2 + L_3) + \frac{1}{\mathrm{j}\omega(C_2 + C_3)} \end{cases} \tag{11}$$

The input power of the system is:

$$P_{in} = \frac{U_{in}^2 \left(Z_{2\_sea} + \Delta Z_2 + \Delta Z_3\right)}{\omega^2 M_{sea}^2 + (Z_{1\_sea} + \Delta Z_1)(Z_{2\_sea} + \Delta Z_2 + \Delta Z_3)} \tag{12}$$

The output power of the system is:

$$P_{out} = \frac{(\omega M_{sea} \dot{U}_{in})^2 R_L}{\left[\omega^2 M_{sea}^2 + (Z_{1\_sea} + \Delta Z_1)(Z_{2\_sea} + \Delta Z_2 + \Delta Z_3)\right]^2} \tag{13}$$

System efficiency is:

$$\eta = \frac{P_{in}}{P_{out}} = \frac{(\omega M_{sea})^2 R_L}{(Z_{2\_sea} + \Delta Z_2 + \Delta Z_3)[(Z_{1\_sea} + \Delta Z_1)(Z_{2\_sea} + \Delta Z_2 + \Delta Z_3) + (\omega M_{sea})^2]} \tag{14}$$

Similarly, when the system operates under resonance conditions, that is, $L_1 = L_2 = L_3$; $C_1 = C_2 = C_3$, and the resonance condition $\mathrm{j}\omega L + \frac{1}{\mathrm{j}\omega \mathrm{C}} = 0$ is satisfied, the maximum transmission efficiency of the system can be simplified as:

$$\eta_{\max} = \frac{\omega^2 M_{sea}^2 R_L}{(R_2 + R_L + \Delta Z_2 + \Delta Z_3) \times [(R_1 + R_{\mathrm{B}} + \Delta Z_1)(R_2 + R_L + \Delta Z_2 + \Delta Z_3) + \omega^2 M_{sea}^2]} \tag{15}$$

4. EXPERIMENTAL VERIFICATION OF THE MODEL SUGGESTED

To verify the accuracy of the proposed model, a mid-range transmission experiment at a distance of 30 cm was conducted using the experimental platform described in Section 3, as shown in Figs. 3 and 4.

The complex impedance and mutual inductance parameters in the underwater wireless power transfer (UWPT) model are obtained using the open-circuit method on the secondary side, where key quantities are experimentally measured, and the corresponding parameters are calculated in a seawater environment. The extracted values are then substituted into the original Kirchhoff's voltage equations to predict the load voltage of the system. Finally, the accuracy and applicability of the proposed model are validated by comparing the predicted results with experimental measurements.

Taking the 1RX model as an example, the open-circuit method on the secondary side is adopted to experimentally obtain the complex impedance. Accordingly, Equation (10) is modified as Equation (16), as shown below.

$$\begin{bmatrix} \dot{U}_{in} \\ \dot{U}_2 \end{bmatrix} = \begin{bmatrix} Z_1 + \Delta Z & j\omega M_{sea} \\ j\omega M_{sea} & Z_2 + 2 * \Delta Z \end{bmatrix} \cdot \begin{bmatrix} \dot{I}_1 \\ 0 \end{bmatrix} \tag{16}$$

The complex impedance and complex mutual inductance in the equation can then be calculated as follows:

$$\begin{cases} M_{sea} = \frac{\dot{U}_2}{j\omega \dot{I}_1} \\ \Delta Z = \frac{\dot{U}_{in}}{\dot{I}_1} - Z_1 \end{cases} \tag{17}$$

In Equation (17), $\dot{U}_{in}$ represents the input voltage on the primary side, and $\dot{U}_2$ denotes the open-circuit voltage on the secondary side. Since the introduced complex impedance and complex mutual inductance are special parameters that contain imaginary components, all measurements in the circuit are referenced to the phase of the input voltage source.

4.1. Impedance Acquisition

4.1.1. 1RX System Complex Impedance Acquisition

Figure 11 illustrates the frequency-dependent behavior of the magnitude of complex impedance in the 1RX WPT system under seawater conditions. As shown in the figure, the magnitude of the complex impedance remains positive across the entire frequency range, indicating energy losses caused by eddy current in the seawater medium, which are primarily manifested as resistive losses [11, 13].

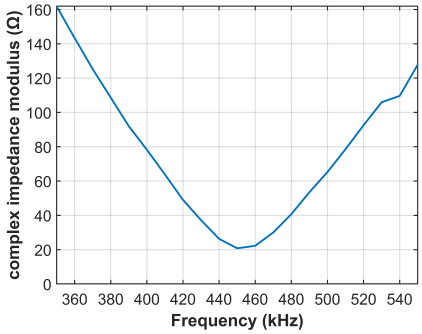

FIGURE 11. Change in complex impedance modulus of 1RX WPT system under seawater.

In addition, the impedance magnitude exhibits a decreasing-then-increasing trend concerning frequency, reaching its minimum near the system's resonant frequency. This observation implies that the energy transfer efficiency is optimized at resonance.

The real part of the complex impedance primarily reflects the resistive components of the circuit. Its value remains positive throughout the entire frequency range, indicating energy loss caused by eddy current. As shown in Fig. 12(a), the frequency-dependent trend of the real part is similar to that of the impedance magnitude: it reaches a minimum near the resonant frequency and generally exhibits a decreasing-then-increasing pattern.

Figure 12(b) presents the variation of the imaginary part of the complex impedance with frequency. Unlike the real part, the imaginary part is positive in the low-frequency region, indicating an inductive characteristic, and becomes negative at higher frequencies, suggesting capacitive behavior. Overall,

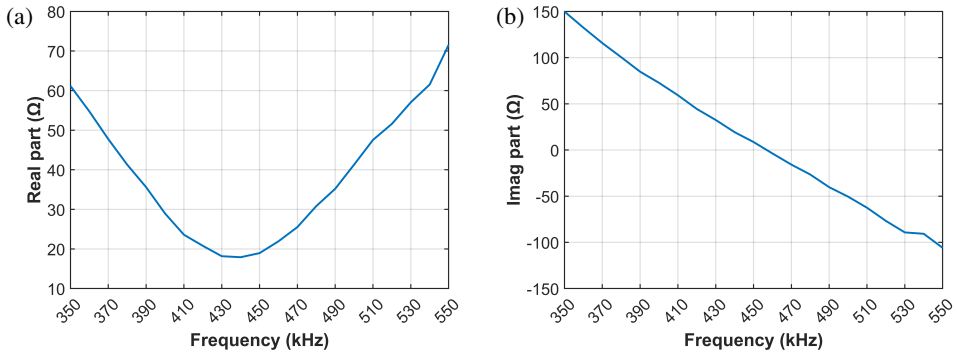

FIGURE 12. Impedance changes of the 1RX WPT system under seawater: (a) real part; (b) imaginary part.

the imaginary part decreases gradually as the frequency increases.

4.1.2. 2RX System Complex Impedance Acquisition

The variation characteristics of complex impedance in the dual-receiver system are consistent with those in the single-receiver system. As shown in Fig. 13, the magnitude of the complex impedance initially decreases and then increases with increasing frequency, reaching its minimum near the system's resonant frequency, which corresponds to the point of maximum transmission efficiency.

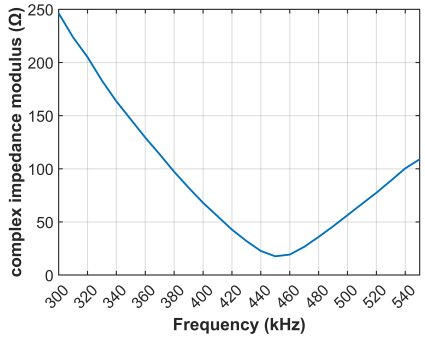

FIGURE 13. Change in complex impedance modulus of the 2RX WPT system under seawater.

Figure 14 illustrates the variation of both the real and imaginary parts of the complex impedance. The real part remains positive throughout the frequency range and follows a similar trend, first decreasing and then increasing, which reflects the change in the resistive component of the circuit.

In contrast, the imaginary part generally decreases with increasing frequency. It is positive in the low-frequency range, indicating inductive characteristics, and becomes negative at higher frequencies, indicating capacitive characteristics. This reveals the complex inductive-capacitive transformation of the system's reactance as the frequency changes.

4.2. Mutual Induction Acquisition

To further investigate the coupling behavior of the system in different media, the mutual inductance of both 1RX and 2RX configurations was experimentally measured in seawater and compared with that in the air.

4.2.1. 1RX System Mutual Complex Induction Acquisition

In an air medium, the magnitude of mutual inductance depends solely on the physical structure of the coils (e.g., wire diameter, number of turns, radius) and their relative positioning (including distance, axial alignment, and offset angle). Once the coil parameters and transmission distance are fixed, the mutual inductance remains constant. However, in a seawater environment, mutual inductance becomes frequency-dependent and exhibits noticeable variation with frequency [11].

This frequency-dependent behavior of mutual inductance is further confirmed through experimental measurements.

As shown in Fig. 15, the magnitude of the complex mutual inductance measured in a seawater medium shows an overall increasing trend with rising frequency, with the growth becoming more evident in the high-frequency range.

Figure 16 shows that both the real and imaginary parts of the complex mutual inductance increase as frequency rises. The real part remains positive across the frequency range, indicating effective magnetic coupling between coils in seawater. Meanwhile, the imaginary part varies with frequency, being negative at low frequencies and turning positive at higher frequencies, which reflects the increasing eddy current losses with frequency.

In addition, compared to the air environment, the real part of the mutual inductance in seawater is larger, indicating that seawater enhances magnetic coupling under midrange transmission conditions. This enhancement reflects the impact of the conductive medium on the magnetic field distribution and energy transfer characteristics between the coils.

4.2.2. 2RX System Mutual Complex Induction Acquisition

Unlike complex impedance, the complex mutual inductance in the 2RX model shows notable differences compared to the 1RX model. As shown in Fig. 17, its magnitude increases with frequency and remains consistently positive. However, unlike the 1RX model, which exhibits a rapid increase in the low-frequency region, the 2RX model demonstrates a slower

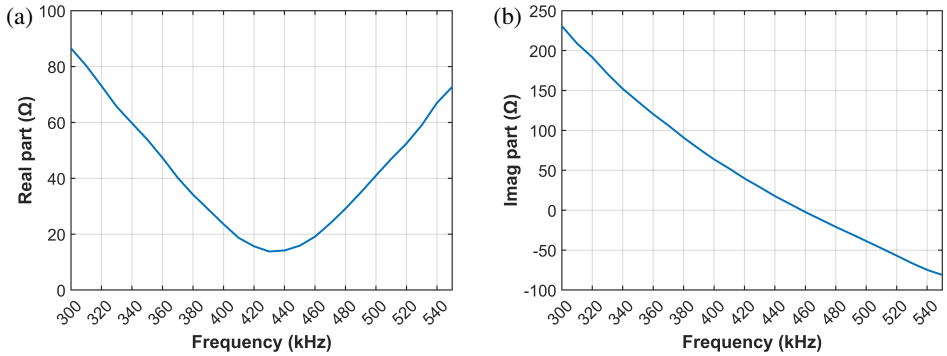

FIGURE 14. Impedance changes of the 2RX WPT system under seawater: (a) real part; (b) imaginary part.

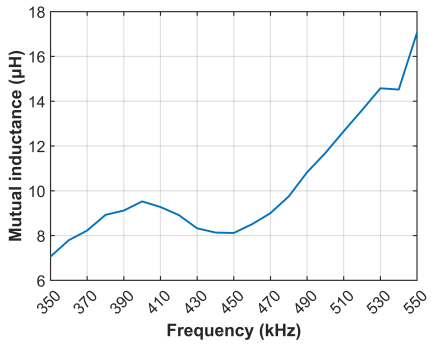

FIGURE 15. Change in mutual inductance modulus of the 1RX system under seawater.

growth at low frequencies, with the increase becoming more pronounced in the high-frequency range.

A closer examination of the trends in the real and imaginary parts of the complex mutual inductance, as illustrated in Fig. 18, shows that the real part in the 2RX model exhibits a similar trend to the magnitude. In the low-frequency region, the variation in the real part is minimal, but it gradually increases with frequency and remains consistently positive throughout the frequency range.

In contrast, the imaginary part shows a declining trend at high frequencies and remains negative across the entire frequency spectrum, indicating a persistent inductive loss behavior under the 2RX configuration.

4.3. Load Voltage Prediction and Experimental Verification

4.3.1. Prediction of the Load Voltage at Seawater

To verify the accuracy of the complex impedance and complex mutual inductance measured in the experiment, the calculated complex impedance and complex mutual inductance are substituted into the original circuit model equation to predict the load-end voltage, which is then compared with the actual load voltage measured in the experiment. As shown in Fig. 19, the calculated prediction results and the experimental measurement values show good agreement at an intermediate transmission distance (approximately 30 cm).

4.3.2. Load Voltage Prediction of the 2RX System at Variable Balancing Resistor R_B

Experimental results indicate that the 2RX system achieves higher transmission efficiency than the 1RX configuration under midrange conditions in seawater. However, due to the use of a symmetrical circuit — specifically, the addition of a balancing resistor R_B on the primary side — the overall system efficiency remains relatively low. In practical applications, the value of the balancing resistor should be minimized to enhance energy transfer performance.

By varying the value of the primary-side balancing resistor, a noticeable improvement in efficiency was observed [24]. Specifically, when R_B was reduced from 20 Ω to 1 Ω, the maximum efficiency increased from approximately 12% to about 25%. In addition, the predicted load voltage based on the proposed complex impedance and mutual inductance model shows good agreement with the experimental results, as illustrated in Fig. 20.

4.4. Efficiency Improvement Explanation

As introduced in Section 2, the parameter α is used to characterize the improvement in transmission efficiency. A larger α corresponds to higher efficiency.

For the 2RX WPT system, the primary and secondary side currents can be calculated using Equation (10) and are expressed as follows:

$$\begin{cases} \dot{I}_1 = \dfrac{\dot{U}_{in}(Z_2+\Delta Z_2+\Delta Z_3)}{\omega^2 M_{sea}^2+(Z_1+\Delta Z_1)(Z_2+\Delta Z_2+\Delta Z_3)} \\ \quad = \dfrac{\dot{U}_{in}}{Z_1+\Delta Z_1+\frac{(\omega M_{sea})^2}{Z_2+\Delta Z_2+\Delta Z_3}} \\ \dot{I}_2 = \dfrac{\omega M_{sea}\dot{U}_{in}}{\omega^2 M_{sea}^2+(Z_1+\Delta Z_1)(Z_2+\Delta Z_2+\Delta Z_3)} \end{cases} \tag{18}$$

Accordingly, the parameter α_{2RX} can be calculated. Similarly, α_{1RX} can also be obtained. Based on the ratio $\alpha_{2RX}/\alpha_{1RX} > 2.07$, with a maximum value of approximately 21.23, it can be concluded that the underwater 2RX system achieves significantly higher transmission efficiency than the 1RX configuration.

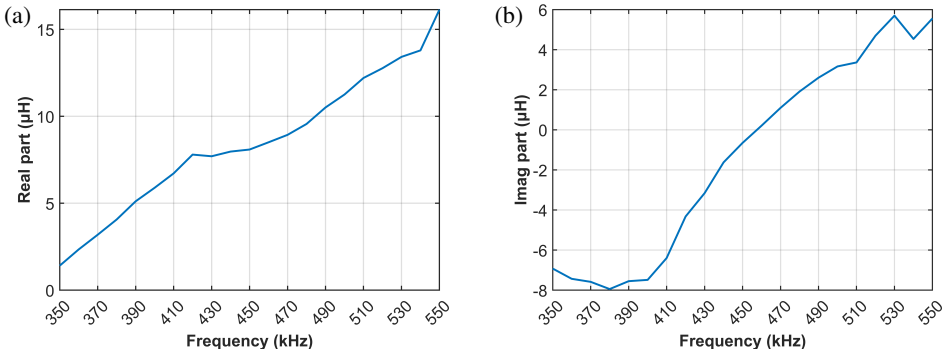

FIGURE 16. Changes in the mutual inductance of the 1RX system under seawater: (a) real part; (b) imaginary part.

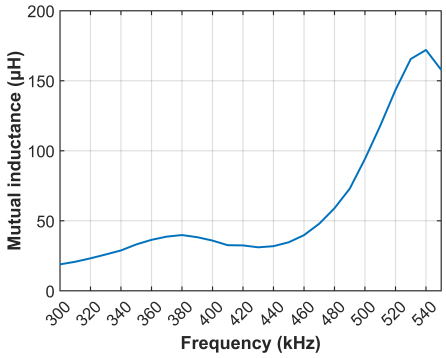

FIGURE 17. Change in mutual inductance modulus of the 2RX system under seawater.

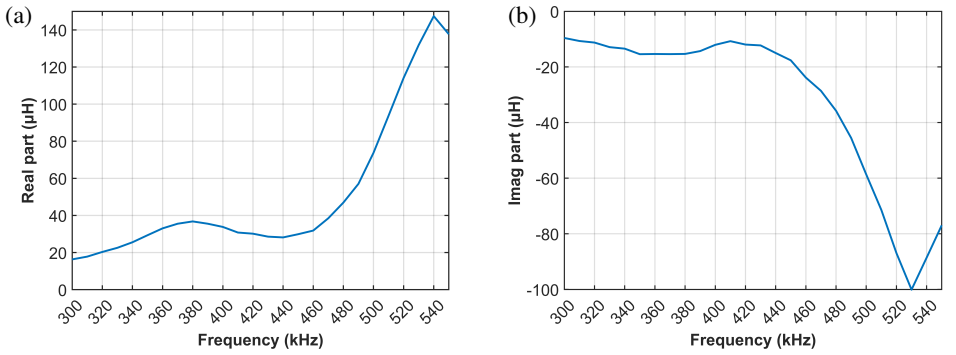

FIGURE 18. Changes in the mutual inductance of the 2RX system under seawater: (a) real part; (b) imaginary part.

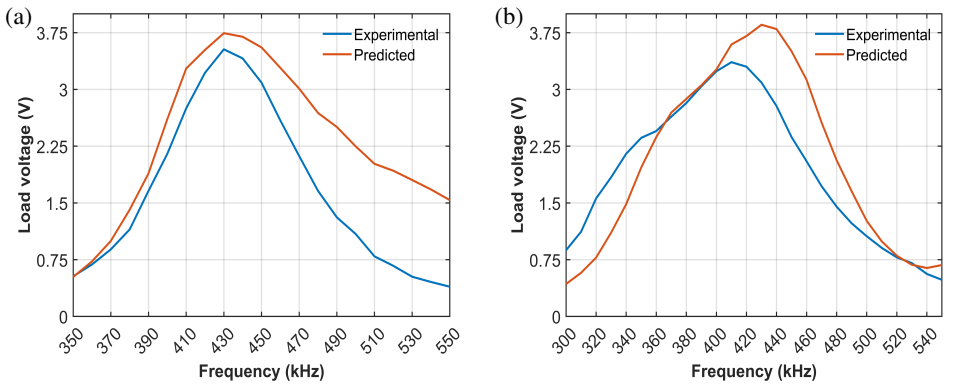

FIGURE 19. Load voltage prediction: (a) 1RX; (b) 2RX.

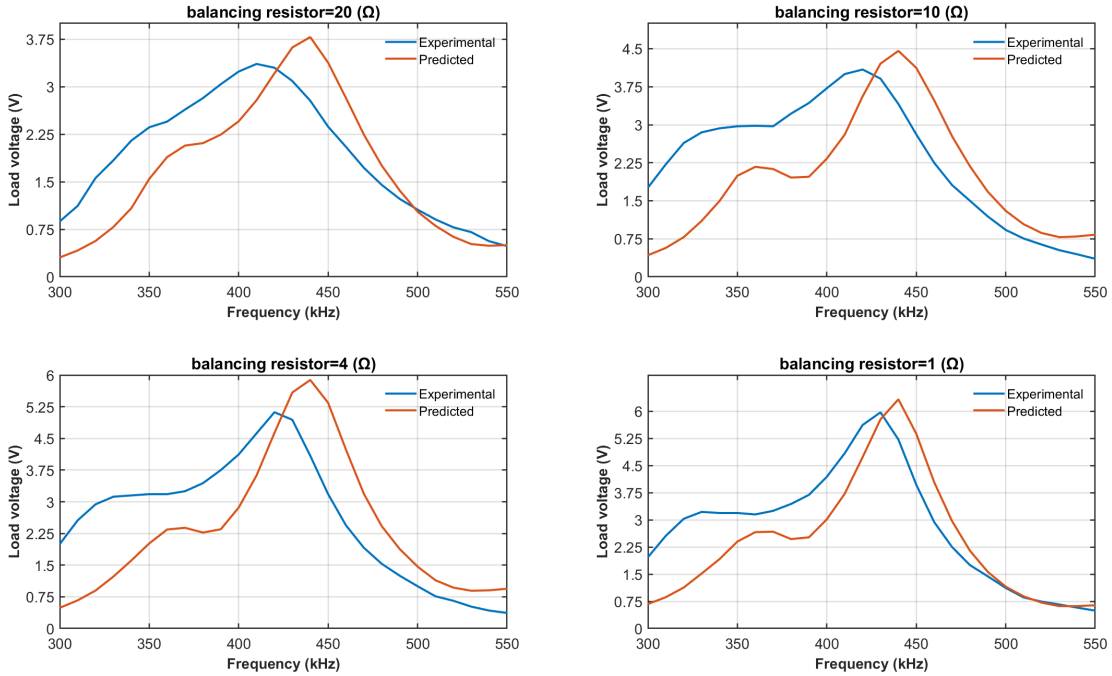

FIGURE 20. Variable balance resistor load voltage prediction.

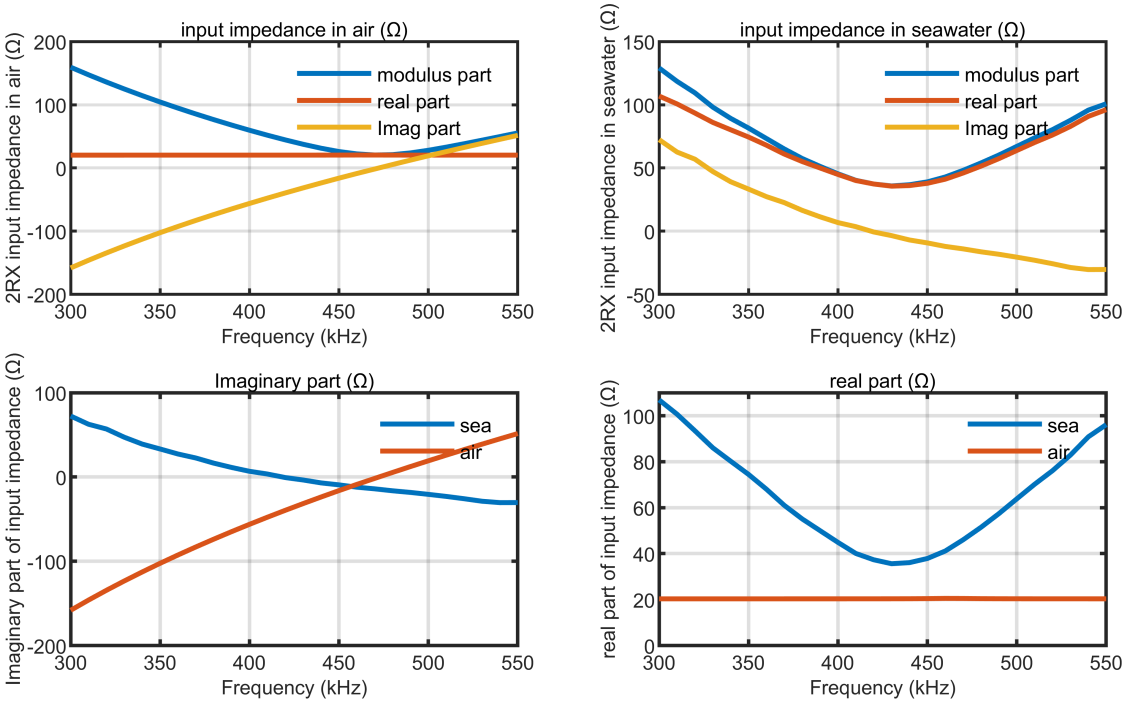

FIGURE 21. Input impedance of the 2RX system in air and seawater.

4.5. Resonant Frequency Shift Analysis

As shown in Fig. 9, experimental results indicate that in a seawater environment, the frequency corresponding to the maximum load voltage of the 2RX system shifts leftward to approximately 420 kHz compared to that in air [25].

In Section 3, the overall input impedance of the system, including the reflected impedance $Z_{ref} = \frac{(\omega M_{12}+M_{13})^2}{Z_2}$ is derived by calculating the primary and secondary side currents. The input impedance in air and seawater is denoted as $Z_{in\_air} = Z_{1\_air} + \frac{(\omega(M_{12}+M_{13}))^2}{Z_{2\_air}}$ and $Z_{in\_sea} = Z_{1\_sea} + \frac{(\omega M_{sea})^2}{Z_2+\Delta Z_2+\Delta Z_3}$. Z_{1_air} and Z_{1_sea} are

shown in formula (2) and formula (11) respectively.

As previously discussed, the efficiency reaches its maximum when the current ratio α is maximized. Similarly, the load voltage also reaches its peak when the system's input impedance is minimized. In the 2RX configuration with a 20 Ω balancing resistor, the input impedance of the system in both air and seawater is shown in Fig. 21.

In air, the system's self-inductance and compensation capacitance remain constant, resulting in a fixed resonant frequency, which can be theoretically calculated using theformula $f = \frac{1}{\sqrt{L_i C_i}} (i = 1, 2)$. Based on this calculation, the resonant frequency corresponding to the maximum load voltage of the 2RX system in air is approximately 460 kHz. This theoretical value shows good agreement with the frequency at which the input impedance reaches its minimum, and the imaginary part of the input impedance becomes zero, as illustrated in Fig. 21.

In seawater, however, due to the medium's unique electrical properties, the resulting input reactance reaches zero near 420 kHz, indicating a shift in the resonant frequency. Similarly, as shown in Fig. 21, the resonant frequency in seawater also occurs near 420 kHz when the input impedance reaches its minimum and its imaginary part becomes zero. This observation aligns well with the analysis in air and explains the leftward shift of the maximum load voltage frequency in the seawater environment.

5. SUMMARY

In this paper, the transfer characteristics of 1TX2RX WPT systems in seawater have been systematically investigated, with comparative analysis against the 1TX1RX configuration. By introducing complex impedance and complex mutual inductance into the theoretical model, the key influence of the seawater environment on transmission performance is clarified.

The main conclusions are as follows:

(1) Enhanced transmission performance:

The 1TX-2RX system demonstrates higher load voltage and transmission efficiency at a midrange transmission distance of 30 cm compared with the 1TX-1RX system. Moreover, it maintains stable operation under coil misalignment, showing superior robustness in seawater conditions.

(2) Accurate modeling with complex parameters:

A circuit model incorporating complex impedance and complex mutual inductance is proposed. The predicted load voltage matches well with experimental results, confirming the model's validity for seawater WPT analysis.

(3) Distinct frequency response of multi-receiver systems:

Compared with the 1RX configuration, the 2RX system exhibits unique frequency response characteristics. The complex mutual inductance increases more significantly, highlighting the potential advantages of multi-coil systems in complex media.

This research provides both theoretical insights and experimental evidence for marine wireless energy replenishment and intelligent underwater device power supply. Future work will focus on combining electromagnetic field simulations and transmission channel modeling to further reveal the coupling mechanisms of underwater WPT in complex media.

REFERENCES

[1] Hui, S.-Y. R., Y. Yang, and C. Zhang, "Wireless power transfer: A paradigm shift for the next generation," *IEEE Journal of Emerging and Selected Topics in Power Electronics*, Vol. 11, No. 3, 2412–2427, 2023.

[2] Orekan, T. and P. Zhang, *Underwater Wireless Power Transfer: Smart Ocean Energy Converters*, 1st ed., Springer, 2019.

[3] Lee, S. B. and I. G. Jang, "Coil layout optimization for maximizing the power transfer efficiency of wireless power transfer systems with multiple transmitter coils," *IEEE Journal of Emerging and Selected Topics in Power Electronics*, Vol. 8, No. 3, 2672–2681, 2020.

[4] Oshimoto, N., K. Sakuma, and N. Sekiya, "Improvement in power transmission efficiency of wireless power transfer system using superconducting intermediate coil," *IEEE Transactions on Applied Superconductivity*, Vol. 33, No. 5, 1–4, 2023.

[5] Lei, Y., J. Zhang, K. Song, G. Wei, C. Zhu, and C. C. Chan, "Stability analysis of multi-load inductively coupled power transfer system," *Transactions of China Electrotechnical Society*, Vol. 30, 187–192, 2015.

[6] Deng, Z., H. Hu, Y. Su, F. Chen, J. Xiao, C. Tang, and T. Lin, "Design of a 60-kW EV dynamic wireless power transfer system with dual transmitters and dual receivers," *IEEE Journal of Emerging and Selected Topics in Power Electronics*, Vol. 12, No. 1, 316–327, 2024.

[7] Yang, L., X. Chen, J. Sun, L. Tian, Z. Bu, D. Xing, Y. Zhang, B. Feng, H. Wen, Y. Zhao, T. Yang, J. Huang, D. Zhu, A. Zhang, and X. Tong, "High power and high freedom platform type undersea wireless power transfer station without ferrite core for AUVs," *IEEE Journal of Emerging and Selected Topics in Power Electronics*, Vol. 13, No. 1, 1269–1280, 2025.

[8] Kim, J.-W., H.-C. Son, D.-H. Kim, K.-H. Kim, and Y.-J. Park, "Analysis of wireless energy transfer to multiple devices using CMT," in *2010 Asia-Pacific Microwave Conference*, 2149–2152, Yokohama, Japan, 2010.

[9] Yoon, I.-J. and H. Ling, "Investigation of near-field wireless power transfer under multiple transmitters," *IEEE Antennas and Wireless Propagation Letters*, Vol. 10, 662–665, 2011.

[10] Mai, R. and L. S. Ma, "Research on inductive power transfer systems with dual pick-up coils," *Proceedings of the CSEE*, Vol. 36, No. 19, 5192–5199, 2016.

[11] Zhang, K., Y. Ma, Z. Yan, Z. Di, B. Song, and A. P. Hu, "Eddy current loss and detuning effect of seawater on wireless power transfer," *IEEE Journal of Emerging and Selected Topics in Power Electronics*, Vol. 8, No. 1, 909–917, 2020.

[12] Mese, H. and M. A. Budak, "Efficiency investigation of a 400 W resonant inductive wireless power transfer system for underwater unmanned vehicles," in *2020 IEEE Wireless Power Transfer Conference (WPTC)*, 223–226, Seoul, Korea (South), 2020.

[13] Kim, J., K. Kim, H. Kim, D. Kim, J. Park, and S. Ahn, "An efficient modeling for underwater wireless power transfer using *Z*-parameters," *IEEE Transactions on Electromagnetic Compatibility*, Vol. 61, No. 6, 2006–2014, 2019.

[14] Hasaba, R., K. Okamoto, S. Kawata, K. Eguchi, and Y. Koyanagi, "Magnetic resonance wireless power transfer over 10 m with multiple coils immersed in seawater," *IEEE Transactions on Microwave Theory and Techniques*, Vol. 67, No. 11, 4505–4513, 2019.

[15] Sun, P., X. S. Wu, J. Cai, X. N. Wang, X. C. Zhang, Y. Liang, Q. Xiong, and E. G. Rong, "Eddy current loss analysis and frequency optimization design of double-sided LCC-IPT system in seawater environment," *Science China Technological Sciences*, Vol. 65, No. 2, 407–418, 2022.

[16] Chu, S., M. S. Luloff, J. Yan, P. Petrov, C. J. Stevens, and E. Shamonina, "Magnetoinductive waves in attenuating media," *Scientific Reports*, Vol. 11, No. 1, 7679, 2021.

[17] Niu, W., X. Yu, and W. Zhang, "Experimental results and analysis of midrange underwater wireless power transfer," *International Journal of Circuit Theory and Applications*, Vol. 51, No. 6, 2674–2688, 2023.

[18] Xu, J., X. Li, H. Li, Z. Xie, and Q. Ma, "Maximum efficiency tracking for multitransmitter multireceiver wireless power transfer system on the submerged buoy," *IEEE Transactions on Industrial Electronics*, Vol. 69, No. 2, 1909–1919, 2022.

[19] Gan, L. and W. Niu, "Experimental results and analysis of a 2-transmitter wireless power transfer system in seawater at midrange," *Electrical Engineering*, Vol. 106, No. 5, 5885–5895, 2024.

[20] Niu, W.-Q., J.-X. Chu, W. Gu, and A.-D. Shen, "Exact analysis of frequency splitting phenomena of contactless power transfer systems," *IEEE Transactions on Circuits and Systems I: Regular Papers*, Vol. 60, No. 6, 1670–1677, 2013.

[21] Hu, S. and W. Niu, "Experimental results and analysis of wireless charging technology for equipment under seawater," *World Electric Vehicle Journal*, Vol. 16, No. 4, 195, 2025.

[22] Wang, J., B. Song, and Y. Wang, "A method to reduce eddy current loss of underwater wireless power transmission by current control," *Applied Sciences*, Vol. 12, No. 5, 2435, 2022.

[23] Wang, S., W. Niu, and X. Zhou, "Modeling wireless power transfer in marine environment via integrated electromagnetic field and circuit analysis," *Measurement*, Vol. 251, 117224, 2025.

[24] Chen, Y., W. Niu, Y. Yang, and Y. Amirat, "Experimental results and analysis of midrange underwater asymmetric wireless power transfer," *Journal of Marine Science and Engineering*, Vol. 12, No. 4, 567, 2024.

[25] Hu, S. and W. Niu, "Analysis on the resonant frequency of wireless power transfer system in seawater," *Electrical Engineering*, Vol. 107, 13 423–13 435, 2025.